Supporting Information

Palladium Nanoparticles with High Energy Facets as a Key Factor of Dissociating O_2 in the Solvent-Free Selective Oxidation of Alcohols

Feifei Wang, [a] *Zhansheng Lu,* [b] *Lin Yang,* [*a] *Yanxing Zhang,* [b] *Qinghu Tang,* [a] *Yuming Guo,* [a] *Xiaoming Ma*[a] *and Zongxian Yang*[b]

a School of Chemistry and Chemical Engineering, Key Laboratory of Green Chemical Media and Reactions, Ministry of Education, Henan Normal University, Xinxiang 453007, P.R. China

b College of Physics & Information Engineering, Henan Normal University, Xinxiang 453007, P.R. China

1. Experimental Section

Chemicals. Sodium hydroxide (NaOH), glutamate, ethylene glycol, ethanol and sodium borohydride ($NaBH_4$) were purchased from the China National Pharmaceutical Group Corp. Palladium chloride ($PdCl_2 \cdot 2H_2O$) was purchased from Alfa Aesar. Benzyl alcohol (99%), DL-sec-phenethylalcohol (98%), 4-methoxybenzyl alcohol (98%) and cinnamyl alcohol (98%) were all purchased from Beijing Innochem Science & Technology Co., Ltd. Aladdin Reagent Company. All chemicals were analytical grade and were used without further purification. Double distilled water (DD water) was used in all of the experiments.

Main experiment for preparation of Pd/F-HAP catalyst. HAP [$Ca_{10}(PO_4)_6(OH)_2$] with a flower-like three dimensional architecture (F-HAP) was successfully prepared through a facile transformation process of hedgehog-like aragonite precursors according to our previous report.[1] A detailed process of catalyst preparation was as follows: an aqueous solution of $PdCl_2$ (2 mg/mL, 1.5 mL), and glutamate (50 mg) were mixed together in EG (35 mL). The pH of the system was adjusted to ca. 10 by dropwise addition of the 8 wt% NaOH/EG solution under vigorous stirring. During the process, the yellow solution turned into colorless. Subsequently, F-HAP (1g) was added, and the mixture was stirred for 0.5 h to obtain a homogeneous suspension. Upon completion, the suspension was transferred into a 50 mL Teflon-lined stainless steel autoclave.

The autoclave was sealed, heated at 80℃ for 8 h, and air-cooled to room temperature. Finally, the product was collected by centrifugation and washed several times with double distilled water. The obtained product was dried at 40℃ under vacuum for 8 h and denoted as Pd/F-HAP.

Control experiment for preparation of Pd/F-HAP catalyst. As a comparison, a control experiment that prepares Pd/F-HAP-*control* catalyst with $NaBH_4$ as reducing agent was performed. A detailed process was as follows: F-HAP (1g), sodium citrate (50 mg) and an aqueous solution of $PdCl_2$ (2 mg/mL, 1.5 mL) were added in 50 mL ethanol–water (1:1, v/v) solution, and kept stirring for 1 h. A freshly prepared solution of $NaBH_4$ (50 mg in 50 mL DD water) was added dropwise into the above solution under stirring for 2 h to form Pd nanocrystals, and then the stirring was continued for another 10 h to make sure the completely decomposition of the redundant $NaBH_4$. Finally, the product was collected by filtration and washed several times with DD water and ethanol, then dried at 40 ℃ in vacuum condition for 12 h.[2] The catalyst was named Pd/F-HAP-*control*.

Characterization. Powder X-ray diffraction (XRD) measurements were performed with a Cu Ka radiation source to determine the crystal phase of the Pd particles. Particle characteristics such as shape and size were determined by high-resolution transmission electron microscopy (HRTEM). The field-emission scanning electron microscopy (FE-SEM) images and the EDAX mapping analysis were used to study the uniform distribution of Pd nanoparticles. The compositions of the Pd/F-HAP catalysts were evaluated by inductively coupled plasma-mass spectrometry (ICP-MS) analysis. The specific surface area of F-HAP samples was detected by a BET surface area analyzer (ASAP-2020, Micromeritics In strument Corp., USA) via the nitrogen-adsorption method. In-situ X-ray absorption fine structure (XAFS) experiments were performed in a transmission mode at the BL14W1 XAFS station in the Shanghai Synchrotron Radiation Facility (SSRF, PR China).

Catalytic reaction. The catalytic oxidation of alcohols was carried out using a batch-type reaction vessel equipped with a reflux condenser. The procedure was as follow: A certain amount of catalyst was added into the alcohol, and the mixture was heated to the reaction temperature under vigorous stirring. Then the O_2 gas flow was bubbled into the mixture to start the reaction. After the reaction, the solid catalyst was filtered off and the liquid products were analyzed by gas chromatography after adding dodecane as the internal standard.[3] Moreover, the application scope of the Pd/F-HAP for four common alcohols was examined.

Recyclability of Pd/F-HAP catalyst. The recycling tests of the Pd/F-HAP catalyst for the solvent-free aerobic oxidation of DL-sec-phenethylalcohol were studied. The catalyst was recovered after each reaction run, washed with DD water, dried at 313 K under vacuum and reused in a subsequent new catalytic run. As shown in Fig. S2, the conversion and selectivity towards acetophenone are essentially constant in the consecutive runs. This verifies that the catalyst can be used in recycles.

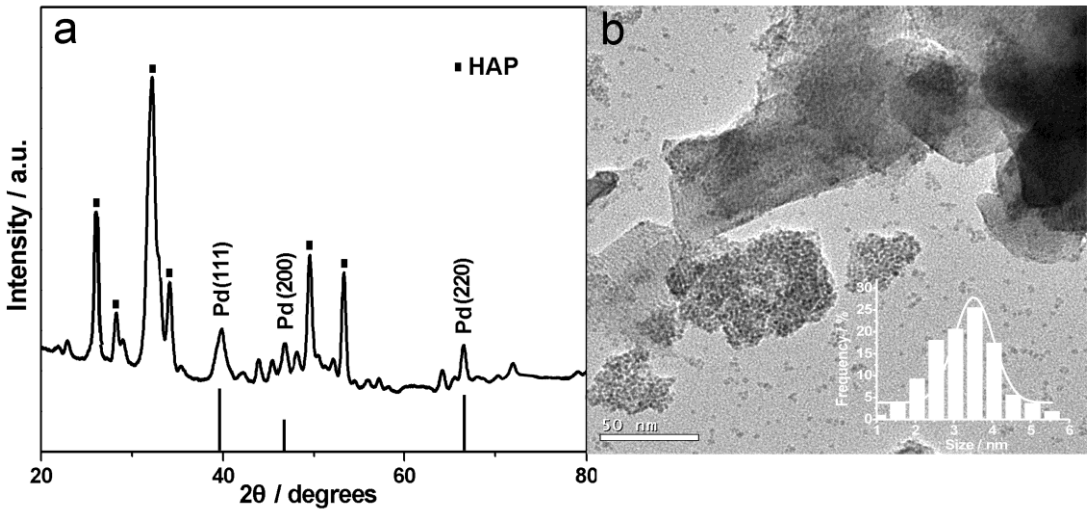

Fig. S1. (a) XRD pattern of Pd/F-HAP-*control* catalyst. The black vertical lines indicate the peak positions of the fcc palladium reflections (JCPDF card, 01-1310). (b) TEM image of Pd/F-HAP-*control*, inset: corresponding size distribution histograms of Pd/F-HAP-*control*)

Table S1. BET specific surface area of different types of HAP

sample	BET surface area (m^2/g)	Ref.
F-HAP	238.1	
HAP from natural bone materials	87-100	4
hollow HAP microspheres	164.7	5
HAP nanocrystals	137	6

BET analysis of N_2 adsorption data, determined at liquid nitrogen temperature, resulted in specific surface areas (m^2/g) of 238.1 for F-HAP, compared to 87-100 m^2/g for natural bone minerals, 164.7 m^2/g for hollow HAP microspheres, and 137 m^2/g for HAP nanocrystals. Thus, the present results reveal that F-HAP which maintains a high surface area is beneficial to the improvement of the catalytic activity of the Pd/F-HAP catalyst.

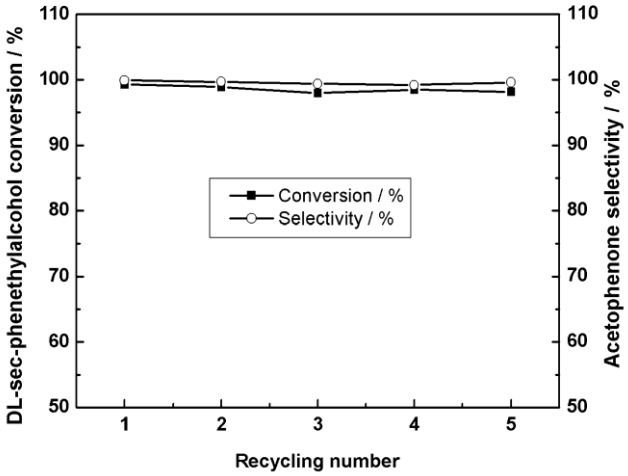

Fig. S2. Recycling of Pd/F-HAP catalyst in the solvent-free aerobic oxidation of DL-sec-phenethylalcohol. Conditions: catalyst = 0.1 g; DL-sec-phenethylalcohol = 5ml; O_2 flow rate = 12 cm^3min^{-1}; T = 403 K; reaction time = 1.5h.

2. Computational Details

Spin-polarized calculations were performed by the VASP code with the generalized gradient approximation (GGA) of the Perdew-Burke-Ernzerhof (PBE) form.[7-9] The projector augmented wave (PAW) method [10]combined with a plane wave basis and cutoff energy of 400 eV was used to describe core and valence electrons. In all calculations, O_2 was adsorbed on one side of the slab only, and except those of the bottom layer of the slab, all the atoms were allowed to move in structural optimization (force threshold was 0.01 eV/Å). The Brillouin-zone integrations were performed with a 4 × 4 × 1 Monkhorst–Pack grid and a Gaussian smearing parameter, sigma = 0.2 eV.[11,12] The structures were optimized until the force on each atom was less than 0.01 eV /Å.

The electronic structure and bonding features were analyzed by means of the Bader-type atomic charges[13] and the electron localization functions (ELF).[14] ELF plots provide a measure of electron localization in space (e.g., as in a covalent bond) and will help to characterize the nature of the interaction between the adsorbed O_2 and the Pd surfaces. Bader's "atoms in molecules" theory was used to assign charges to atoms and fragments. These charges provide useful clues to how the charges transfer between different atoms or fragments.

The adsorption energy (E_{ad}) was calculated as:

$$E_{ad} = - [E(O_2/support)-E(support)-E(O_2)] \quad (1)$$

where E (support), E (O_2) and E (O_2/support) are the total energies of the optimized bare Pd surface, a gaseous O_2 molecular atom and the optimized O_2/Pd system for the same support, respectively. Theoretically, positive adsorption energy denotes a stable adsorption structure. The O_2 dissociation barriers were calculated with the climbing image nudged elastic band (cNEB) method in the transition-state (TS) search[15,16] using the same convergence criterion as in the geometry optimizations)

Pd surfaces models. From XRD pattern (Fig. 2), the Pd nanoparticles formed on the F-HAP present three facets, including {110}, {100} and {111}. The model Pd particle (including 36 Pd atoms, Pd_{36}) on HAP {211} was built to represent the Pd nanoparticles formed on the F-HAP support, as shown in Fig. S3. When Pd_{36} is adsorbed on HAP {211}, the negligible negative charges of the Pd particles (0.19 |e|) are found from the Bader-type charge analysis. As a test, a smaller Pd particle (including 16 Pd atoms, Pd_{16}) is put on HAP {211} and the Pd particle gets 0.13 |e|, which is also negligible. Thus the effect of the HAP support on the charge of the Pd particles is negligible.

In the following calculations, three Pd facets are built to investigate the adsorption properties of the O_2 on the Pd/F-HAP systems. The Pd {110}, {100} and {111} facets were modeled as the periodic slabs including five atomic layers and a vacuum layer larger than 13 Å. For Pd {111} and {100}, a 3×3 expansion of the surface cell was utilized, and the Pd {110} was modeled by a 2×3 surface cell. These sizes of the vacuum layer and the cell expansions largely eliminate the interactions among the adsorbed O_2 in neighbouring surface cells.

The adsorption and dissociation of the O_2 on Pd faces. Here, the adsorption properties of the O_2 adsorbed on the Pd {110} facets is presented as representation for that of the O_2 adsorbed on Pd {110}, {100} and {111} facets. According to our investigation on the interaction between O_2 and the Pd facets, the similar adsorption properties were found for O_2 adsorbed on different facets.

One of the stable O_2 adsorption configurations on the Pd {110} facets is presented in Fig. S4a. Firstly, the molecular O_2 stays on the hollow site of four Pd surface atoms, and each of the O atoms in O_2 bonds to two Pd atoms, respectively, resulting in an E_{ad} of 1.15 eV. The adsorbed O_2 was negatively charged by 0.79 |e|, indicating the formation of the O_2^-. The formation of the O_2^- is also confirmed by the ELF map (Fig. S4b). For the dissociative adsorption of O_2, one of the stable adsorption configurations for the two atomic O adatoms on Pd {110} facets is presented in Fig.

S4c. The two O adatoms are negatively charged by ~ 0.80 |e|, forming two O^{-}. The calculated dissociative adsorption energy of O_2 is 1.69 eV. Similar adsorption properties of the O_2 were also found on Pd {100} and {111} facets.

The dissociation barriers of O_2 are calculated based on the cNEB method in the TS search. The calculated O_2 dissociation barriers for O_2 on Pd {110}, {100} and {111} facets are 0.18, 0.12 and 0.66 eV respectively, which demonstrate that the high energy facets {110} and {100} are of benefit to O_2 dissociation. Fig. S5 presents the initial states (IS) and final states (FS) as well as their corresponding transition states (TS) with the barriers. The rather small dissociation barriers (< 0.2 eV) indicate that the O_2 dissociation on the {110} and {100} facets are very easy, even at low temperature. Thus the O_2 dissociation on {110} and {100} facets would be the key to the alcohol oxidation.

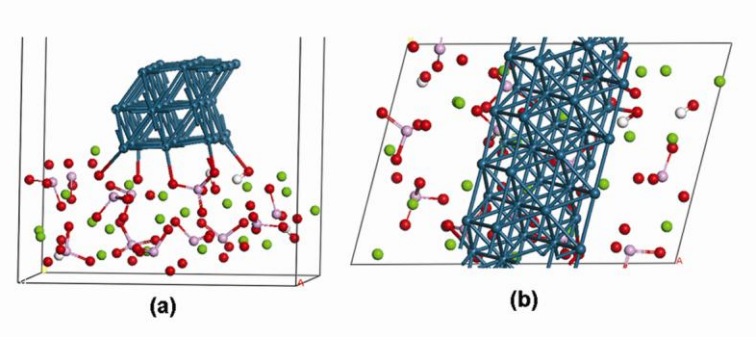

Fig. S3. The model of Pd particles (Pd_{36}) supported on the HAP. (a) Side view, (b) Top view.

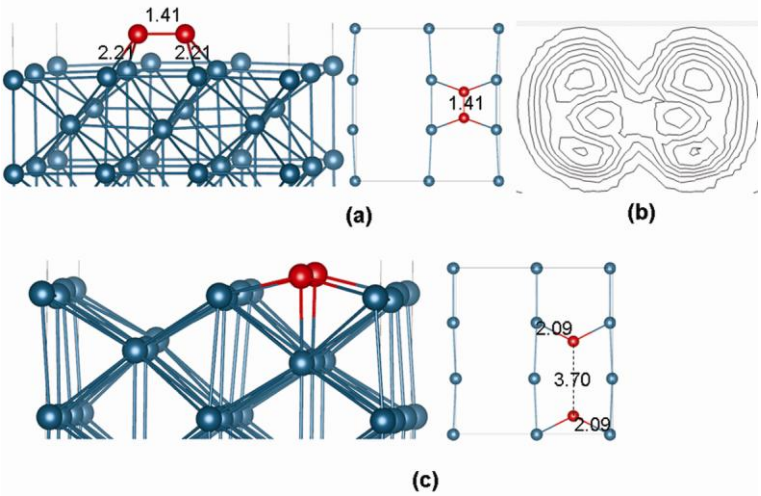

Fig. S4. The optimized O^2 adsorption configuration on the Pd {110} facets (a) The adsorption of the O_2 on Pd {110} faces, (b) contours of the electron localization function (ELF) in a vertical plane passing through O–O bond, (c) The dissociative adsorption configuration of O_2 on Pd {110} facets.

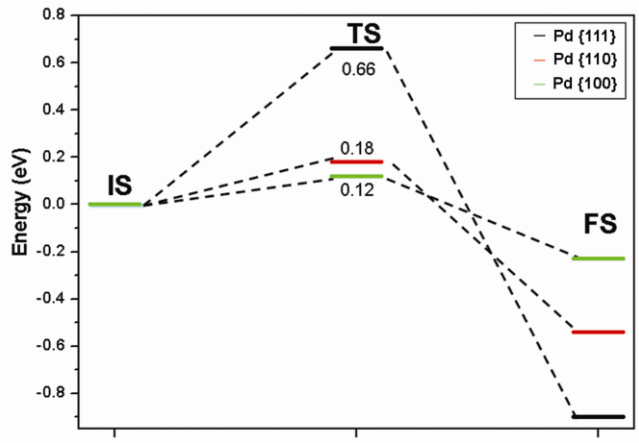

Fig. S5. The potential energy surface for O_2 dissociation on Pd {111}, {110} and {100} facets.

3. Pd K-edge XANES of palladium references and HAP-supported palladium catalyst

The XANES represents an electronic transition state from inner electronic level to outer unoccupied levels and contains the information of chemical environment and bonding surrounding the X-ray absorbing atom. Fig. S6 shows Pd K-edge XANES spectra for Pd references and the Pd/F-HAP catalysts. The maximum of the absorption edge in each spectrum corresponds to the allowed 1s → 5 p transition, merging into the continuum at higher energies. Pd foil had a distinctly different shape (Fig. S6a) in XANES spectra compared to Pd oxide (Fig. S6b). Palladium supported on F-HAP showed a similar spectrum (Fig. S6c) to Pd foil, indicating that Pd^{2+} was well reduced to Pd nanoparticles. For the Pd/F-HAP catalyst soaked in oxygen for 1.5 h under room temperature, the shape of the XANES spectrum (Fig. S6d) was identical to that of the Pd oxide but differed from that of the Pd foil. This reveals that all Pd species are in the oxidation state under the action of oxygen. In Fig. S6e, the spectrum of the recovered Pd/F-HAP for the oxidation of DL-sec-phenethylalcohol was similar to that of the palladium foil.

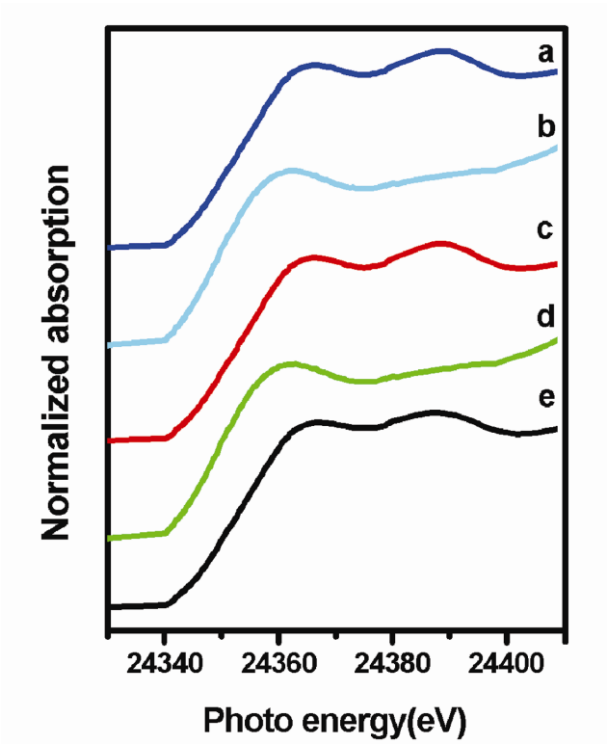

Fig. S6. Pd K-edge XANES of palladium references and HAP-supported palladium catalyst: (a) Pd foil, (b) Pd oxide, (c) Pd/F-HAP, (d) Pd/F-HAP in oxygen 1.5 h under room temperature and (e) recovered Pd/F-HAP for the oxidation of DL-sec-phenethylalcohol

References

1 F. Wang, Y. Guo, H. Wang, L. Yang, K. Wang, X. Ma, W. Yao, H. Zhang, *CrystEngComm.*, 2011, **13**, 5634-5637.

2 Z. Bai, L. Yang, J. Zhang, L. Li, C. Hu, J. Lv, Y. Guo, *J. Power Sources*, 2010, **195**, 2653-2658.

3 Q. Tang, T. Liu, Y. Yang, *Catal. Commun.*, 2008, **9**, 2570-2573.

4 N. V. Wood, *Science*, 1947, **105**, 531-532.

5 S. Jiang, Q. Yao, G. Zhou, S. Fu, *J. Phys. Chem. C*, 2012, **116**, 4484−4492.

6 M. Tagaya, S. Motozuka, T. Kobayashi, T. Ikoma, J. Tanaka, *Ind. Eng. Chem. Res.*, 2012, **51**, 11294−11300.

7 G. Kresse, J. Furthmuller, *J. Comput. Mater. Sci.*, 1996, **6**, 15-50.

8 G. Kresse, J. Hafner, Phys. Rev. B: Condens. *Matter Mater. Phys.*, 1994, **49**, 14251-14269.

9 J. P. Perdew, J. A. Chevary, S. H. Vosko, K. A. Jackson, M. R. Pederson, D. J. Singh, C. Fiolhais, Phys. Rev. B: Condens. *Matter Mater. Phys.*, 1992, **46**, 6671-6687.

10 P. E. Blöchl, Phys. Rev. B: Condens. *Matter Mater. Phys.*, 1994, **50**, 17953-17979.

11 H. J. Monkhorst, J. D. Pack, Phys. Rev. B: Condens. *Matter Mater. Phys.*, 1976, **13**, 5188-5192.

12 M. Methfessel, A. T. Paxton, Phys. Rev. B: Condens. *Matter Mater. Phys.*, 1989, **40**, 3616-3621.

13 G. Henkelman, A. Arnaldsson, H. Jónsson, *J. Comput. Mater. Sci.*, 2006, **36**, 354-360.

14 B. Silvi, A. Savin, *Nature*, 1994, **371**, 683-686.

15 G. Henkelman, B. P. Uberuaga, H. J. Jónsson, *Chem. Phys.*, 2000, **22**, 9901-9904.

16 G. Henkelman, H. J. Jónsson, *Chem. Phys.*, 2000, **113**, 9978-9985.